THE UNIVERSITY OF MICHIGAN

COLLEGE OF LITERATURE, SCIENCE, AND THE ARTS
Department of Physics

Technical Report No. 11

ELASTIC SCATTERING OF NEGATIVE PIONS BY PROTONS AT 2 BEV/C

D. E. Damouth
L. W. Jones
M. L. Perl

ORA Project 03106

under contract with:

DEPARTMENT OF THE NAVY
OFFICE OF NAVAL RESEARCH
CONTRACT NO. Nonr-1224(23)
WASHINGTON, D.C.

administered through:

OFFICE OF RESEARCH ADMINISTRATION ANN ARBOR

June 1963

engn
UHR 0593

This report was also a dissertation submitted in partial fulfillment of the requirements for the degree of Doctor of Philosophy in The University of Michigan, 1963.

ACKNOWLEDGMENTS

We would like to acknowledge the help of C. C. Ting who was largely responsible for the design of the apparatus and made many contributions to the analysis of the data.

R. Y. Y. Lee, O. Haas, and K. W. Lai provided much help in setting up and running the experiment.

The experiment could not have been performed without the enthusiastic support of Dr. E. J. Lofgren, his colleagues, and the Bevatron staff.

TABLE OF CONTENTS

LIST OF TABLES

LIST OF FIGURES

ABSTRACT

The negative pion-proton differential elastic cross section at an incident pion momentum of 2 Bev/c has been measured in a spark chamber experiment. Approximately 7000 events were obtained in the center of mass angular range $.95 > \cos \theta^* > -.97$.

The data show an approximately exponential diffraction peak which when extrapolated to $\cos \theta^* = 1.0$ is consistent with the optical theorem prediction. A second peak, with a maximum of .23 mb/sr is seen at $\cos \theta^* = .2$. The backward scattering is not isotropic, but drops smoothly from .12 mb/sr at $\cos \theta^* = 0$ to about .01 mb/sr at the most backward angles.

An analysis in terms of a simple diffraction model and a fit in powers of $\cos \theta^*$ are given.

I. INTRODUCTION

A. PION-NUCLEON SCATTERING

The importance of the study of pion-nucleon interactions lies in the light it sheds on the nature of the basic forces which act between elementary particles. In particular, the ability to calculate the angular distribution and dependence on incident momentum of elastic scattering will be a powerful test of any theory which attempts to describe these forces, and it is therefore very desirable to obtain accurate experimental knowledge of this interaction.

Interest in the energy region around 2 Bev comes from several sources. Data available up to now at this energy has been severely limited by poor statistics and large measurement errors. A luminescent chamber experiment at this energy suggested some structure, possibly oscillatory, in the large angle region, although definite conclusions could not be made.[1] Recently a peak has been discovered in the π^--p total cross section at about 2 Bev, and the possible connection between this peak and the appearance of structure in the large angle elastic scattering is very interesting.[2]

Although successful fundamental theories are still lacking, the elastic scattering angular distributions can be at least qualitatively explained in terms of an "optical model," which is easily visualized and from which straightforward calculations of the cross sections can be made.

In this approach, particle scattering is treated as though it were a potential scattering problem. If one considers a plane wave incident on a spherically symmetric potential, the scattering amplitude may be expressed on terms of the familiar partial wave expansion

$$A(\theta) = \frac{1}{2iK} \sum_{\ell=0}^{\infty} (2\ell+1)(\alpha_\ell \, e^{2i\delta_\ell} - 1) P_\ell(\cos\theta)$$

where α_ℓ may be thought of as an absorption coefficient and δ_ℓ is called the phase shift of the ℓth partial wave. The phase shifts and absorption coefficients completely determine the scattering and for a given potential may always be calculated, although this may be very tedious. If the extent of the potential can be measured by a radius, a, then it is easily shown that the phase shifts will be small for $\ell \gg Ka$. Thus, this partial wave expansion is most useful for small values of Ka. In fact, for very low energies, one can easily show that the only significant contribution is from $\ell = 0$, giving isotropic scattering.

In terms of the above partial wave expansion, one may write[3]

$$\left.\frac{d\sigma(\theta)}{d\Omega}\right)_{\text{elastic}} = |A(\theta)|^2$$

$$\sigma_{\text{total inelastic}} = \frac{\pi}{K^2} \sum_{\ell} (2\ell+1)(1-|\alpha_\ell|^2)$$

$$\sigma_{\text{total elastic}} = \frac{\pi}{K^2} \sum_{\ell} (2\ell+1)\,|1-\alpha_\ell|^2$$

At 2 Bev, $K_{cm} = 4.4 \times 10^{13}$ cm^{-1} and a is found to be about 10^{-13} cm. Thus Ka = 4.4 and partial waves up to an ℓ of at least this large must be considered. The large number of partial waves involved at this energy makes this type of analysis of rather limited utility.

When large numbers of partial waves are important, i.e., for Ka $\gg$ 1, another approach is often used. One simply assumes that all partial waves for $\ell < L$ are completely absorbed and that for all partial waves with $\ell > L$ there is no absorption. This model is chosen because of its extreme simplicity, and contains only one parameter, the number of partial waves absorbed. Alternatively, one can write $L = Kr_0$ and use the parameter r_0, which should in some sense represent the geometric size of the scatterer.

For this model, one can write with no further approximations

$$A(\theta) = \left(\frac{i}{2K}\right)\left[P'_{L+1}(\cos\theta) + P'_L(\cos\theta)\right]$$

$$\sigma_{total} = 2\pi\lambda^2(L+1)^2$$

$$\sigma_{inelastic} = \pi\lambda^2(L+1)^2 = \sigma_{elastic}$$

One may use similar optical models with more parameters to obtain better agreement with experiment. Greider and Glassgold[4] introduced a model in which the transition from absorption to non-absorption occurs over a range of ℓ values and the phase, δ_ℓ, is allowed to vary in a simple way. For scattering of elementary particles from each other, attempts to fit data with these more sophisticated many parameter diffrac-

tion models are of questionable utility since they shed little light on the nature of the fundamental interactions.

A recent attempt at a more basic theory is based on a transformation of the partial wave expansion proposed by Regge[5] with subsequent generalization to the high energy relativistic problem.[6]

It is possible to rewrite the partial wave expansion of the scattering amplitude for potential scattering as a sum of residues at "Regge Poles" in the upper half of the complex angular momentum plane plus terms which under suitable conditions are negligible. These poles are found to move through the plane as a function of energy and the scattering amplitude shows a resonance behavior whenever one of these poles crosses lines in the plane on which the real part of the angular momentum is integer. For $E < 0$, one obtains bound states, while for $E > 0$ resonances occur, for a given pole, at either all even or all odd integer values of the real part of the momentum variable. Recently, theoreticians have assumed that this non-relativistic formalism can be carried over to the relativistic problem, and further assumed that the resonances correspond to observable particles. The resonances of a given pole would form a family of particles all with the same values of isotopic spin, Baryon number, strangeness, etc.

This, together with additional assumptions, makes possible the calculation of scattering amplitudes for various high energy processes and in particular, for elastic scattering, where recent theories based on this formalism predict that the diffraction peak should be roughly ex-

ponential and should become narrower with increasing energy. This behavior is seen in P-P scattering. For π-p scattering, the peak is roughly exponential, but apparently does not become narrower. In fact, the width appears to be almost constant from below 2 Bev up to at least 17 Bev.[7]

The experimental consequences of these theories have all been derived as high energy approximations. It is not expected that the simple Regge behavior will be seen at energies as low as 2 Bev. If the theory can make specific predictions here, they will probably be quite complicated.

Many of the difficulties inherent in calculating elastic scattering cross sections disappear in the case of forward scattering. It is easily shown that, under very general conditions, the relation

$$\sigma_{tot} = \frac{4\pi}{K} \text{ Im}[f(0)]$$

must hold, where f(0) is the elastic scattering amplitude in the forward direction and K is the propagation vector of the incident particle in the center of mass system.

The real part of the forward scattering amplitude can be calculated from dispersion relations, given a knowledge of the total π^- and π^+ cross sections for all energies. This is not very accurate, since the total cross sections are not well known, but Re f(0) is small compared to Im f(0) so that f(0) is still well determined. One obtains

$$|f(0)|^2 = |\mathrm{Re}[f(0)]|^2 + |\mathrm{Im}[f(0)]|^2 = \left(\frac{K}{4\pi}\sigma_{tot}\right)^2 + |D|^2$$

and at 2 Bev,

$$\frac{d\sigma(0)}{d\Omega} = 16.1 \text{ mb/sr} .$$

The validity of the partial wave analysis and of a simple diffraction model for the data at 2 Bev/c will be discussed in Section VI. To the extent possible, the data will be analyzed in terms of these models. The calculated point at cos θ^* = 0 will be compared to the value obtained by extrapolating the observed data back to this point.

B. SURVEY OF EXISTING EXPERIMENTAL DATA

The π^--p total cross section is shown in Fig. 14. The peak at 2 Bev seems to be well established, although it has only recently been discovered, and almost nothing is known about the mechanism responsible for it.

The differential cross section for energies below 1.5 Bev has been considered in detail elsewhere.[8] Above 1.5 Bev, the existing data are summarized in Table I. The 1.5 Bev data for both π^- and π^+ gives a fairly good measurement of the large angle differential cross section. However, above this energy the large angle cross section becomes much smaller and is not well determined. In fact, little more than an upper limit has been obtained.

The spark chamber π^+ data at 1.5, 2.0, and 2.5 Bev/c and the lum-

inescent chamber π^- data at these energies did not extend far enough into the diffraction peak to determine its shape well or to allow accurate extrapolation to the optical theorem point at cos θ^* = 1.0.

The results which may be compared directly to the data presented in this dissertation are the luminescent chamber large angle experiment at 2 Bev/c, the unpublished bubble chamber data of Erwin and Walker at 1.89 Bev/c and the scintillation counter data of Cook, et al., at 1.95 Bev/c. The results of these experiments are presented and compared in Section VI.

II. EXPERIMENTAL EQUIPMENT AND PROCEDURE

A beam of 2 Bev/c negative pions derived from the Bevatron of Lawrence Radiation Laboratory struck a liquid hydrogen target. An elastic scattering of a beam particle in the target was detected by an array of scintillation counters and coincidence electronics which produced a signal whenever a set of particles coming out of the target approximately satisfied the appropriate kinematics. This event signal triggered a set of spark chambers which were placed so as to accurately determine the trajectories of the incident and scattered pion and the recoil proton. The spark chambers were then photographed and the particle trajectories measured by hand from the photographs.

A. BEAM AND MAGNETS

The beam layout is shown in Fig. 1. The circulating proton beam struck an internal copper target; negative pions thus produced were deflected out of the Bevatron by its magnetic field through a thin window in the vacuum tank. The momentum of the pion beam was partially analyzed by the magnetic field of the Bevatron and two C-magnets. Two quadrupole triplets with an 8 in. aperture focused the emerging beam, which was then momentum analyzed by an 18 x 36 in. H-magnet.

A scintillation counter telescope, consisting of counters C10 and C11 selected pions from the beam which were within a 2 in. diam circle at the upstream end of the LH_2 target and whose paths were within 1° of

being parallel to the beam axis.

B. HYDROGEN TARGET

The hydrogen target used in this experiment is shown in Fig. 2. Liquid hydrogen at atmospheric pressure was contained in a .007 in. Mylar bag, 18 in. long and 3.5 in. in diam, with approximately hemispherical ends. This bag was suspended with its longitudinal axis lying along the beam axis. In order to provide the necessary thermal insulation, the target was contained in a thin (.032 in.) aluminum vacuum chamber. Radiation barriers consisting of 10 layers of .0005 in. aluminized Mylar interleaved with 10 layers of .001 in. aluminum foil further reduced the thermal flux into the target. The beam entered the vacuum chamber through a thin Mylar window. The target was filled by gravity from an overhead reservoir.

C. EVENT DETECTION SYSTEM

The location of the scintillation counters is shown in Fig. 3. The portion of the beam to be used was defined by counters C10 and C11, a gas threshold Cerenkov counter, and anti-coincidence counter A4. A coincidence between C10 and C11 defined a particle which passed through a 2 in. diam circle defined by C11 at an angle of less than 1° to the beam axis. Counter A4 contained a 2 in. diam hole through which the beam passed and served to reduce accidental coincidences. Elastic events were recognized by requiring that at least one particle emerge from the

target on each side of the beam axis at an angle of less than ±30° to a horizontal plane through the target. Thus, counters C6, C5, C8 subtended an angle of approximately ±30° to the horizontal on one side of the target and similarly C7, C4, C9, subtended ±30° on the other side. Counter A1, located in the beam downstream from the target and connected in anti-coincidence, helped to further reduce triggering by inelastic events and by chance coincidences of particles or noise pulses. This counter, when placed in coincidence with the beam telescope, provided a measure of the total number of beam particles which were scattered less than 2°. This was a convenient check on the operation of the equipment.

Anti-coincidence counters A2 and A3 served to reject some events in which an extra non-coplanar charged particle was produced. These counters are not shown in Fig. 3 since they cover the area between the coplanarity counters above and below the hydrogen target.

The shape of the coplanarity and beam counters is indicated in Fig. 6. All counters except C11 were 0.5 in. commercial polystyrene-based scintillation material and were coupled to 6810A phototubes by lucite light pipes. Counter C11 was sufficiently close to the hydrogen target so that an effort was made to minimize its interaction with the beam. Thus the scintillation material was only 0.125 in. thick. To reduce the possibility of beam counts arising from Cerenkov radiation in the lucite light pipes, this light pipe consisted only of a thin reflecting cylinder of aluminum filled with air.

The construction of the gas Cerenkov counter is described else-

where.[9] It was filled with sulfur hexafluoride to a pressure such that it would count pions but reject slower (heavier) particles. By recording the rate of coincidences of the Cerenkov counter with the beam telescope as a function of pressure in the Cerenkov counter, an estimate of the electron content of the beam was obtained.

Block diagrams of the electronics are shown in Figs. 4 and 5. An event was recorded whenever one or more of the right coplanarity counters and one or more of the left coplanarity counters and the beam telescope all triggered, while none of the anti-coincidence counters triggered, all within the resolution time of the coincidence circuits.

Prior to the experiment, each scintillation counter with its photo-tube was individually checked. Curves of supply voltage vs. counting rate were obtained, and with the counter operating on its plateau the characteristic delay between the incidence of a particle and the output pulse was measured. This delay and the time difference due to the large path lengths traversed by particles between the various counters were compensated for by the inclusion of suitable delay lines between the counters and the coincidence circuits.

The entire array of counters was rechecked after the experiment was completely setup in its final position, to verify that the correct time delays were used. At intervals during the experiment the counters were individually checked with a small beta source.

Except as noted below, the electronic circuits used were standard units supplied by the Bevatron. This equipment is described in detail

in the Lawrence Radiation Laboratory Counting Handbook,[10] so only a brief description follows. The coincidence circuits had a minimum resolution time of about 5 ns. Clipping lines 5 ns long were used, giving a resolution of approximately 10 ns. This number was chosen to be slightly larger than the maximum time spread expected from the counters.

The pulse splitters shown in Fig. 4 were transistor emitter follower units which introduced essentially no attenuation or delay. The first decade of the scalars for the beam, transmitted beam and monitor had a resolution time of about 100 ns, while the event and coplanarity scalars used units of about 1.0 μs resolution. The average beam rate was about 30,000 pions, spread fairly uniformly over 0.3 sec, giving about 10 μs per particle so that corrections for accidental coincidences or for lost pulses in the scalars are negligible. The gating circuits are shown in Fig. 5. The Berkeley scalar gate was triggered by a pulse from the Bevatron. It then generated a gate signal which turned the Berkeley scalars on for a time interval which could be adjusted to coincide with the desired portion of the beam spill.

The "event pulses" from the coincidence logic were fed to a "self-canceling gate." This circuit was turned on by the Berkeley scalar gate and then transmitted the first event pulse to the camera advance system, spark chamber pulser, and "stop event" scalar, at which time it turned off, gating off the Eldorado scalars, for a time interval long enough to allow the spark chambers to recover and long enough to close camera "A" and open camera "B." After this interval (adjustable, but

typically 50 ms) the self-canceling gate turned on, gating on the Eldorado scalars, and transmitted the next pulse to occur after which it turned off again. This cycle was repeated until the Berkeley scalar gate turned off, at which time the self-canceling gate and the Eldorado scalars were also turned off.

Since it was desirable to photograph only two events per pulse, one on each camera, the gates normally were adjusted so that only two events could be transmitted to the spark chamber pulser during each beam pulse. For example, with a Berkeley scalar gate duration of 180 ms and a self-canceling gate dead time of 100 ms at most two events could be transmitted by the self-canceling gate. On the average, about 10 events per pulse occurred so that two photographs were taken nearly every pulse.

The Berkeley scalars counted continuously for the duration of the Berkeley scalar gate signal. The Eldorado scalars counted only during the time that the spark chamber and camera system was ready to record an event, i.e., not during the dead time of these units. The ratio of event counts to beam counts should, except for statistical fluctuations, be the same for the Berkeley and Eldorado scalars. This was observed to be true.

The monitor system shown in Fig. 4 was connected to a small scintillation counter telescope which looked at the internal Bevatron target from inside the Bevatron shielding, completely independent of the main beam system. Thus it provided a counting rate proportional to the internal beam intensity and dependent upon the manner in which the Bev-

atron was being operated, but entirely independent of the rest of the experimental setup. The ratio of the monitor counting rate to the main beam counting rate should be constant, and any trouble with the beam magnets or counters would show up as a change in this ratio.

D. SPARK CHAMBERS AND ASSOCIATED EQUIPMENT

The details of spark chamber operation and construction have been described elsewhere.[11] Nine spark chambers were used, ranging in size from 8 x 18 in. active area down to 4 x 4 in. Each chamber consisted of seven .001 in. hard aluminum plates, spaced by .375 in. The plates were stretched on lucite frames. Alternate plates were connected together externally to two electrodes, one of which was grounded. The chambers were fired in the usual manner, that is, by charging a capacitor (about .002 μf per chamber) to approximately 12 kv and then, upon the occurrence of an event pulse, discharging the capacitor via an hydrogen thyratron into the chamber. The delay between the event and the firing of the chambers was about 250 ns. A clearing field of about 100 v/cm was maintained across the gaps to sweep out ionization, resulting in a resolution time of the order of 1 μs. The chambers were filled with neon with a small admixture of helium. A flow of a few cc/min of neon was maintained through all chambers, thus keeping the chambers at a slight positive pressure. Recovery time, i.e., the time necessary to sweep ions from the chamber after it is fired, was not carefully investigated, but is of the order of 10 ms.

Since the resolution time of the chambers was short compared to the average interval between beam particles, extra tracks from beam particles not connected with the event were seldom seen.

E. OPTICS AND CAMERA

The spark chambers were each viewed parallel to their plates through two perpendicular faces, giving 90° stereo information. All images were placed on a single 1-1/2 in. strip of 35 mm film by a group of front surface mirrors. The central chambers were viewed through a 36 in. diam 30 ft focal length field lens placed close to the chambers.

Two Beattie Coleman cameras, with 12 in. focal length lenses were located about 30 ft from the central spark chambers. Camera "A" looked straight at the system. Camera "B" was perpendicular to camera "A" and looked into a small front surface mirror placed at 45° to the optical axis adjacent to the lens of camera "A" so that the optical axes of the cameras were as close together as possible. There was, however, a small difference in optical path length, and probably a slight difference between the focal lengths of the two lenses, which resulted in a difference of about 2% in image magnification between the two cameras. Eastman "tri-X" film was used, with the camera lenses stopped down to f/11. The depth of field was sufficient so that little defocusing of the spark images was observed.

III. DATA ANALYSIS

Approximately 30,000 photographs were obtained, of which all were scanned, about half appeared elastic and were measured, and about one quarter were finally accepted as true elastic scattering events.

The scanning and measuring were carried out on machines which projected the film image on an emulsion screen (from behind the screen) at a magnification of about 2/3 actual size. A graduated scale was placed along both edges of each view of each group of chambers. A transparent straight-edge was placed over the track image, and lined up by eye so as to represent the best stright line through the sparks. The intersections of the lines with the scales at the chamber edges were used to define the track coordinates. These intersections were punched on IBM cards.

An IBM 7090 program was written which used the knowledge of the relative positions and magnifications of the spark chambers to reduce the measured track intersections to equations of three straight lines in space, representing the measured trajectories of the incoming pion and outgoing pion and proton.

For an actual elastic event, the beam track would intersect with the two outgoing tracks, all three lying in a plane. Due to measurement error, second scatterings of the outgoing particles, etc., the measured tracks fail to intersect. The intersection was approximately defined as follows: For any pair of straight lines in space, a third straight line

can be found which intersects both of the pair and is perpendicular to each. A measurement along this line gives the minimum distance between the pair of lines, and a point at the center of the segment connecting the pair may be taken as the best estimate of the "intersection" of the two lines.

The minimum separation and intersection were computed in this manner for each of the three possible pairs of the three tracks. The root mean square average of the minimum separations is an indication of the accuracy of the measurement. The three intersections were averaged by a weighted least squares method to determine the best value of the intersection of the three lines. The intersection of each pair of lines was weighted by multiplication with the sine of the angle between the lines, since the accuracy with which the intersection is known is approximately proportional to this quantity (assuming random measurement errors). The root mean square distance between this average intersection and the three intersections of line pairs is another indication of the measurement accuracy.

To check coplanarity, the angle between the incoming track and the plane of the outgoing tracks was computed. For all events which fell within set limits of intersection error and coplanarity error, the program calculated the angles between each outgoing track and the beam track. These two angles, plus an assumption as to identification of the outgoing tracks, are sufficient to kinematically determine the event. Thus,

from the angles the program computed the beam momentum which would yield an elastic event with these angles. This computation was repeated with the opposite identification of outgoing particles. Of the two choices, the one which gives an incident momentum closest to the center of the known beam momentum distribution was accepted as correct. This procedure is justified since at 2 Bev/c the event distribution is not a rapidly varying function of angle in the region around the point where pion and proton angles are equal.

All the parameters mentioned above were punched on cards by the computer, so that the events could later be sorted and summarized according to any desired criteria.

IV. CORRECTIONS TO THE DATA

The significant sources of bias in the experiment and the methods of correcting them are described below.

A. NUCLEAR SCATTERING

In some elastic events one or both of the outgoing particles will undergo a nuclear interaction before being observed in the spark chambers. In nearly every case, this event can no longer be recognized as elastic. The fraction of elastic events lost in this manner can be computed from a knowledge of the pion and proton cross sections on the various materials traversed by the outgoing particles. The path lengths and cross sections are a function both of scattering angle and of position of the interaction in the target. For various scattering angles, the correction was computed as a function of target position and integrated over the target.

B. COUNTER SOLID ANGLE

Of all elastic events with a particular scattering angle occurring in a given region of the target, only a fraction will be oriented so as to trigger the counters. This fraction depends only on the shape and position of the coplanarity scintillation counters and thus can be computed in a straightforward manner. An IBM 7090 program was written which divided the portion of the hydrogen target traversed by the incident

beam into 2304 volume elements and computed, for each volume element, the fraction of events detected as a function of scattering angle. Summing over the volume elements, weighted according to the incident beam distribution, gives the total fraction of events triggering the counters as a function of scattering angle. This curve is shown in Fig. 7 for the entire target and in Fig. 8 for the restricted target region discussed in the next section. The performance of the computer program was checked by manual computation of the corrections for a sample of the volume elements, using an accurate graphical method.

C. SPARK CHAMBER SOLID ANGLE

From certain positions in the target there are particular scattering angles for which elastic events can trigger the scintillation counters without both particles being seen in the spark chambers. A correction is necessary for this type of event, since they were counted by the electronics but could not be measured. This correction is a rapidly varying function of scattering angle and for some angles is greater than 10%. For this reason, the data have been analyzed in two ways. First, all events were used and the above correction made. Second, a restricted target region was used. By using only events from the central 2/3 of the target the above correction, which is large and difficult to obtain accurately, can be eliminated. This is because the effect occurs mainly for events occurring in the ends of the target. It was convenient to calculate this correction together with the nuclear scattering correc-

tion, so that only the combination of the two corrections is plotted. This is shown in Figs. 9 and 10.

D. BACKGROUND EVENTS

The only competing two body final state is in the reaction $\pi^- + p \rightarrow \Sigma^- + K^+$. At 2 Bev/c this cross section is of the order of .02 mb/sr.[12] Taking into account the angular measurement errors, the only overlap between the kinematic curves of this reaction and of elastic scattering occurs in a narrow region centered at a center of mass angle $\cos \theta^* = .81$. This would show as a small bump in the π-p differential cross section at this angle. However, since the π-p cross section is about 1.0 mb/sr at this point, this bump (if it exists) is negligible compared to the statistical errors.

The reactions $\pi^- + p \rightarrow \pi^- p + n\pi$ have a large cross section and may occasionally appear elastic in our pictures. This occurs when two outgoing particles are close to coplanar and the other particles produced are either neutral or do not traverse the spark chambers or anti-coincidence counters. For large angle elastic scattering, the cross section for this background of elastic-appearing events is of the same order of magnitude as the elastic cross section and so must be carefully subtracted. This may be done as follows: Assume that the distribution of the inelastic background as a function of coplanarity error and apparent beam momentum is slowly varying. The distribution of true elastic events as a function of these variables should be an approximately gaussian peak centered at zero in the coplanarity error and at 2 Bev/c in the momentum. Thus the

composite curve of elastic plus inelastic events should be a gaussian peak on top of a slowly varying plateau. The data were fitted to this assumption for various ranges of scattering angle, and the number of events under the plateau was subtracted from the total number of events in each interval.

All events within three standard deviations in coplanarity error and five standard deviations in momentum error were accepted in the final compilation.

E. COULOMB SCATTERING

Calculations show that coulomb scattering is significant only for the slow recoil proton from small angle scattering. Even for these events, the coulomb scattering is less than the angular measurement error so that the only effect is to slightly spread the error distribution for small angles.

F. BEAM ATTENUATION

As the incident beam moves through the traget, particles are removed by interaction with the target so that fewer particles are available to interact at the back of the target than at the front. The effect is simply an overall reduction in effective beam intensity. The effective beam intensity, $\bar{N}$, is given in terms of the incident beam intensity, N, by

$$\bar{N} = \frac{N}{\ell} \int_0^{\ell} e^{-x\rho\sigma}\, dx; \quad \ell = 18 \text{ in.}; \quad \frac{1}{\rho\sigma} = 720 \text{ cm}; \quad \frac{\bar{N}}{N} = .968$$

where ℓ is the target length, σ is the π-p total cross section at 2 Bev/c, and ρ is atoms/cc in liquid hydrogen. The above assumes that other factors are slowly varying functions of target position, so that second order corrections can be neglected.

G. SCANNING EFFICIENCY

During the film scanning and measuring, three different people were employed, using two different scanning machines. The efficiencies were obtained by rescanning some rolls of film and comparing the rescan with the original scan. Several different methods of rescanning were used, as described below.

The first method consisted of a complete and independent rescan and remeasure of some rolls by a different person. Ten rolls were rescanned in this manner, and events missed or mismeasured in the first scan but found in the second were included with events from the first scan in the final compilation.

Another method had the scanners go over previously scanned film simply looking for good events and recording their frame numbers. Subsequently, this list of events was compared with a list of previously measured events. Those events missed in the first scan and found in this rescan were then measured and included in the final compilation. Before this method was employed, some effort was made to correct systematic errors in event identification or measurement.

The third method consisted of remeasuring all events which were rejected by the computer on the basis of the first measurement. This

method should find nearly all measurement errors.

After inclusion of good events found in the various rescans, there is still a residual group of events which were not detected in any of the scans. This can be calculated from a knowledge of the efficiencies of the separate scans, and results in an overall correction factor of 1.019±.006, where the errors are statistical.

H. BEAM MOMENTUM

The momentum analyzing magnets in the beam were set by a wire orbit method to give a momentum of 2 Bev/c at the target. This could be easily checked since for each elastic event the computer calculated a beam momentum. A plot of number of events vs. beam momentum then shows an error distribution peaked at the center of the actual beam momentum distribution. This center is found to be at 2006±10 Mev/c. The spread of momenta in the beam was estimated both by direct calculation and by analysis of the observed error distribution to be about 100 Mev/c.

I. MUON AND ELECTRON CONTAMINATION

From Cerenkov counter pressure curves the electron content of the beam was calculated to be 2.2%. The muon content was estimated to be 6.6%. Since the cross sections of these particles on protons are extremely small, the only correction necessary is to reduce the readings of the beam scalars by the above amounts.

J. COUNTER EFFICIENCY

During a large part of the experiment, coplanarity counter C7 was operating with very low efficiency. This was discovered during data analysis through the presence of a large right-left asymmetry in the number of events at very small scattering angles.

This counter can only trigger for events in the four increments of smallest scattering angle. Therefore, in these increments, only events in which the pion scattered toward the half of the system not containing C7 were used.

V. RESULTS

The differential cross section was calculated by means of the following formula:

$$\left(\frac{d\sigma}{d\Omega}\right)_i = \frac{(n_i - b_i)}{n} \frac{\eta_i}{\Omega_i} \left(\frac{e}{B\alpha\beta}\right) \frac{S}{L\rho 2\pi(\Delta\cos\theta^*)_i}$$

where,

n_i = total number of events in the ith interval which are within three standard deviations of coplanarity

b_i = number of inelastic events in ith interval

n = total number of pictures scanned = 27934

η_i = correction for nuclear interaction of outgoing particles and spark chamber solid angle

Ω_i = effective fraction of solid angle available for detecting event in ith interval

e/B = ratio of number of event coincidence counts to number of incident beam particles = $.890 \times 10^{-2}$

α = correction for muon and electron content of beam = $.912 \pm .02$

β = correction for attenuation of beam = .968

L = target length = 11.57 in. (restricted target volume) or 18 in. (total target volume)

ρ = density of liquid hydrogen in protons per cubic centimeter = 4.196×10^{22}

S = scanning efficiency correction = $1.019 \pm .006$.

This can be written, for the restricted target volume,

$$\left(\frac{d\sigma}{d\Omega}\right)_i = \frac{(n_i - b_i)\eta_i}{\Omega_i(\Delta\cos\theta^*)_i} \cdot 4.7465 \times 10^{-5} \text{ mb/sr.}$$

For the total target volume, the numerical factor becomes 3.0510×10^{-5}.

The results are shown numerically in Table II for the restricted traget and in Table III for the entire target. In order to achieve greatest overall accuracy, the results finally used are a composite of the two sets of data described above.

In the diffraction peak, where statistical accuracy is high, the restricted target results are best, since they minimize the systematic errors. For the large angle portion of the angular distribution, the entire target volume is used since the systematic errors in this data are small compared to the statistical accuracy, and the statistical accuracy is substantially improved by using the entire target volume. The composite results are shown numerically in Table IV and plotted in Figs. 10 and 11.

VI. INTERPRETATION AND CONCLUSIONS

It has become customary to analyze diffraction peaks in terms of a modification of the diffraction model scattering amplitude presented in Section I. There, we wrote

$$A(\theta) = \frac{i}{2K}\left[P'_{L+1}(\cos\theta) + P'_{L}(\cos\theta)\right]$$

under the assumption that the first L partial waves are completely absorbed ($\alpha=0$). To introduce an additional parameter, one assumes

$$\alpha_{\ell} = \alpha\ ; \quad 0 < \alpha < 1$$

for all $\ell \leq L$. This may be thought of as a "grey disc" model where the first L partial waves are attenuated, each by a factor $1-\alpha$, and all other partial waves are unaffected. In terms of this model,

$$A(\theta) = \frac{(1-\alpha)}{2iK}\sum_{\ell=0}^{L}(2\ell+1)P_{\ell}(\cos\theta)$$

$$= \frac{i(1-\alpha)}{2K}\left[P'_{L+1}(\cos\theta) + P'_{L}(\cos\theta)\right]$$

For small scattering angles this expression may be written in the form

$$A(\theta) = (1-\alpha)R\,\frac{J_1(KR\sin\theta)}{\sin\theta}$$

$$\frac{d\sigma}{d\Omega} = \frac{\sigma_{\alpha}}{\pi}\left|\frac{J_1(KR\sin\theta)}{\sin\theta}\right|^2; \quad \sigma_{\alpha} = \pi R^2|1-\alpha|^2$$

The value of R obtained by fitting this equation to the observed angular distribution is a convenient measure of the nuclear size. Figure 12 shows the data together with the above curve plotted for $R = 1.04 \times 10^{-13}$ and $\alpha = .555$. This gives $\sigma_d = 6.72$ and $\sigma_a = 23.5$. This value of R is in good agreement with values found in other experiments over an energy range of 1 to 5 Bev.[13]

The simple grey disc model is used only for convenience. It is not in good agreement with the experimental shape of the diffraction except in a narrow range of angles. A somewhat better fit is obtained with an exponential curve, as shown in Fig. 12. The diffraction peak was fitted by a least squares method in several different angular ranges. The range $.96 \leq \cos \theta^* \leq .88$ as well as a fit to the entire diffraction peak is shown in Fig. 12. A chi-squares test shows that the data for the entire diffraction peak is consistent with a curve of the form

$$\frac{d\sigma(\theta)}{d\Omega} = \frac{d\sigma(0)}{d\Omega} e^{At}$$

where t is the square of the four-momentum transfer, in units of (Bev/c)^2, given by $t = -2p^{*2}(1-\cos \theta^*)$. One finds $d\sigma(0)/d\Omega = 12.78 \pm .45$ mb/sr, $A = 7.94 \pm .16$. From dispersion theory, the forward point is calculated to be $d\sigma(0)/d\Omega = 16.1$ mb/sr, in marked disagreement with the above experimental value. One should note, however, that the fit to the most forward angular region (five points) gives $d\sigma(0)/d\Omega = 15.76 \pm .18$, $A = 9.64 \pm .92$, in agreement with the calculated forward point. There is little

reason to question the calculation of the forward point. The alternatives are either that the diffraction peak becomes narrower and steeper at small angles or that the normalization of the experiment is too low by about 25%. At present this question cannot be resolved.

An approximately exponential diffraction peak is not unreasonable, since it could be explained in terms of a diffraction model with a gaussian scattering density distribution, and also might fit in with theories based on the Regge formalism.

The data have also been fitted with a curve of the form

$$\frac{d\sigma}{d\Omega} = \sum_{\ell=0}^{L} A_\ell \cos^\ell \theta^*$$

using a least squares method. The results are given in Table V for fits both with and without the calculated forward point. The fitting procedure was carried out for various values of L. The value finally chosen is the smallest for which a satisfactory chi-squares test was obtained, and is L = 10 without the forward point or L = 11 including the forward point.

From the diffraction model, partial waves up through the fifth might be expected (KR = 4.4), and the square of $P_5(\cos\theta)$ contains powers of $\cos\theta$ through the tenth. Thus the power series fit is reasonable on the basis of the diffraction model. The fitted curve is shown in Fig. 13. This curve suggests the presence of a very small backward peak. This, however, is probably of little significance.

It is difficult to draw detailed conclusions from the power series fit. In particular, no information is obtained regarding the second peak observed in the angular distribution. If this peak were due to a π^--p resonance, an enhancement of a particular angular momentum state would be expected. Since the diffraction effects make the coefficients of all the terms large, an enhancement of a particular partial wave would be difficult to detect unless it was extremely large. Nevertheless, this interpretation of the secondary peak in terms of a resonance remains very attractive in light of the resonance recently observed in the π^--p total cross section at about 2 Bev/c. It seems likely that the angular distribution will have to be measured at several closely spaced energies in this energy range, and supplemented by additional data such as polarizations, in order to make definitive statements about the effects of such a resonance.

A comparison with previous experiments at this energy is given in Fig. 13. The large angle data of Lai, et al., shows a differential cross section which is larger by at least a factor of two than the data presented here. That experiment suffered from large angular measurement errors, and consequently, the subtraction of inelastic background was very difficult. This may explain their very high differential cross section for the backward angles.

The counter data of Cook, et al., at 1.95 Bev/c for small angles is also shown. Their diffraction peak appears to be too narrow, both on the basis of comparison with the data of this dissertation and comparison

with data at higher and lower energies.

The data of Erwin and Walker at 1.85 Bev/c is also shown in Fig. 13. This was a bubble chamber experiment consisting of about 500 elastic events. The shape of the angular distribution is seen to agree very well with the data presented here, except for the two most forward points. However their normalization is somewhat higher. Integrating over the angular distribution, the data of Erwin and Walker give a total elastic cross section of 8.6 mb while the data presented here give 7.95 mb.

In conclusion, the data shows a roughly exponential diffration peak, consistent with a nuclear "size" of 1.04×10^{-13} cm. This agrees with the values found at higher and lower energies. A second peak is seen in the angular distribution, and can probably be explained in terms of diffraction effects, although it may instead be caused by the resonance which is seen in the total cross section at 2 Bev/c. A decision between these two interpretations is not possible on the basis of this experiment.

The cross section in the backward region is not isotropic, but drops smoothly from 100 ub at $\cos \theta^* = 0$ to approximately 10 ub at $\cos \theta^* = -.8$. There is some evidence for a small narrow backward peak, although this is based on only a few events and is not statistically significant.

TABLE I

A SUMMARY OF PION-PROTON ELASTIC SCATTERING EXPERIMENTS FROM 1.5 TO 3.0 BEV/C

Momentum	Detector	Ref. No.	Number of Events	Angular Range
		Negative Pions		
1.51	luminescent	9	~2400	$-.85 < \cos \theta^* < .74$
1.6		20		
1.85	cloud	16	64	
1.89	bubble	19	536	
1.95	counter	18		$\cos \theta^* > .8$
2.01	luminescent	9	~1300	$-.88 < \cos \theta^* < .81$
2.53	luminescent	9	~1300	$-.86 < \cos \theta^* < .86$
2.8	bubble	17		
3.15	spark	15	~1200	
		Positive Pions		
1.5	spark	14	~1000	
1.69	counter	8	4%	
2.0	spark	14	~1000	
2.5	spark	14	~1000	
2.92	spark	15	~1200	

TABLE II

NUMERICAL RESULTS FOR RESTRICTED TARGET VOLUME

Cos θ^*	Number of Observed Events	Inelastic Background	Number of Elastic Events	$d\sigma/d\Omega$ (mb/sr)	Error (mb/sr)	Cos θ^*	Number of Observed Events	Inelastic Background	Number of Elastic Events	$d\sigma/d\Omega$ (mb/sr)	Error (mb/sr)
.935	446	2	444	6.04	$\pm$.28	.30	56	9	47	.18	$\pm$.03
.925	388	2	386	5.28	$\pm$.27	.26	69	10	59	.23	$\pm$.03
.915	346	2	344	4.74	$\pm$.25	.22	72	9	63	.25	$\pm$.04
.905	284	2	282	3.92	$\pm$.24	.18	56	10	46	.18	$\pm$.03
.890	452	4	448	3.16	$\pm$.15	.14	67	9	58	.23	$\pm$.03
.870	359	4	355	2.54	$\pm$.14	.10	44	8	36	.14	$\pm$.03
.850	297	4	293	2.13	$\pm$.13	.06	47	7	40	.16	$\pm$.03
.83	257	4	253	1.86	$\pm$.12	.02	34	6	28	.11	$\pm$.02
.81	198	4	194	1.45	$\pm$.11	-.02	50	7	43	.17	$\pm$.03
.79	138	3	135	1.02	$\pm$.09	-.06	47	6	41	.16	$\pm$.03
.77	105	2	103	.79	$\pm$.08	-.10	31	7	24	.09	$\pm$.02
.75	85	3	82	.63	$\pm$.07	-.16	56	13	43	.09	$\pm$.02
.73	71	2	69	.54	$\pm$.07	-.24	38	11	27	.05	$\pm$.01
.71	48	3	45	.35	$\pm$.06	-.32	37	8	29	.06	$\pm$.01
.69	33	2	31	25	$\pm$.04	-.40	26	7	19	.03	$\pm$.01
.66	56	5	51	.20	$\pm$.03	-.48	34	6	28	.06	$\pm$.01
.62	41	5	36	.14	$\pm$.03	-.56	23	6	17	.03	$\pm$.01
.58	21	6	15	.06	$\pm$.02	-.64	17	6	11	.02	$\pm$.01
.54	32	6	26	.10	$\pm$.02	-.72	7	6	1	.002	+.01 -.002
.50	20	7	13	.05	$\pm$.02						
.46	27	8	19	.08	$\pm$.02	-.80	7	6	1	.002	+.01 -.002
.42	36	8	28	.11	$\pm$.03						
.38	51	9	42	.17	$\pm$.03	-.88	12	6	6	.01	$\pm$.01
.34	47	10	37	.15	$\pm$.03	-.94	6	3	3	.02	$\pm$.02

TABLE III

NUMERICAL RESULTS FOR TOTAL TARGET VOLUME

Cos θ^*	Number of Observed Events	Inelastic Background	Number of Elastic Events	$d\sigma/d\Omega$ (mb/sr)	Error (mb/sr)	Cos θ^*	Number of Observed Events	Inelastic Background	Number of Elastic Events	$d\sigma/d\Omega$ (mb/sr)	Error (mb/sr)
.935	526	8	518	6.18	$\pm$.28	.34	82	17	65	.17	$\pm$.03
.925	472	7.5	464.5	5.60	$\pm$.26	.30	97	17	80	.21	$\pm$.03
.915	438	7.5	430.5	5.01	$\pm$.25	.26	112	17	95	.25	$\pm$.03
.905	366	7.5	358.5	4.18	$\pm$.22	.22	106	17	89	.23	$\pm$.03
.89	533	14	519	3.04	$\pm$.14	.18	103	17	86	.22	$\pm$.03
.87	433	13	420	2.48	$\pm$.12	.14	102	17	85	.22	$\pm$.03
.85	377	12.5	364.5	2.17	$\pm$.12	.10	61	17	44	.12	$\pm$.02
.83	320	12	308	1.84	$\pm$.11	.06	78	17	61	.16	$\pm$.03
.81	245	11	234	1.40	$\pm$.10	.02	56	17	39	.10	$\pm$.02
.79	177	7	170	1.01	$\pm$.08	-.02	75	17	58	.16	$\pm$.03
.77	138	5	133	.79	$\pm$.07	-.06	68	17	51	.14	$\pm$.03
.75	129	3.5	125.5	.74	$\pm$.07	-.10	49	16.5	32.5	.09	$\pm$.02
.73	97	2	95	.56	$\pm$.06	-.16	80	25	55	.08	$\pm$.02
.71	72	1.5	70.5	.41	$\pm$.05	-.24	58	14	44	.06	$\pm$.01
.69	54	1.5	52.5	.31	$\pm$.04	-.32	49	8	41	.06	$\pm$.01
.66	95	3	92	.27	$\pm$.03	-.40	39	6.6	32.4	.05	$\pm$.01
.62	62	3.5	58.5	.17	$\pm$.02	-.48	42	6.6	35.4	.06	$\pm$.01
.58	38	4	34	.10	$\pm$.02	-.56	30	6.6	23.4	.04	$\pm$.01
.54	38	4.5	33.5	.09	$\pm$.02	-.64	20	6.6	13.4	.02	$\pm$.01
.50	32	5	27	.07	$\pm$.02	-.72	11	5	6	.01	$\pm$.01
.46	44	9	35	.10	$\pm$.02	-.80	11	4.6	6.4	.01	$\pm$.01
.42	55	12	43	.11	$\pm$.02	-.88	16	4.6	11.4	.02	$\pm$.01
.38	83	14	69	.19	$\pm$.03	-.94	8	2.3	5.7	.03	$\pm$.02

TABLE IV

COMPOSITE NUMERICAL RESULTS

Cos θ^*	Number of Observed Events	Inelastic Background	Number of Elastic Events	$d\sigma/d\Omega$ (mb/sr)	Error (mb/sr)	Cos θ^*	Number of Observed Events	Inelastic Background	Number of Elastic Events	$d\sigma/d\Omega$ (mb/sr)	Error (mb/sr)
.935	446	2	444	6.04	$\pm$.28	.34	47	10	37	.15	$\pm$.03
.925	388	2	386	5.28	$\pm$.27	.30	56	9	47	.18	$\pm$.03
.915	346	2	344	4.74	$\pm$.25	.26	69	10	59	.23	$\pm$.03
.905	284	2	282	3.92	$\pm$.24	.22	72	9	63	.25	$\pm$.04
.890	452	4	448	3.16	$\pm$.15	.18	56	10	46	.18	$\pm$.03
.870	359	4	355	2.54	$\pm$.14	.14	67	9	58	.23	$\pm$.03
.850	297	4	293	2.13	$\pm$.13	.10	44	8	36	.14	$\pm$.03
.83	257	4	253	1.86	$\pm$.12	.06	47	7	40	.16	$\pm$.03
.81	198	4	194	1.45	$\pm$.11	.02	34	6	28	.11	$\pm$.02
.79	138	3	135	1.02	$\pm$.09	-.02	75	17	58	.16	$\pm$.03
.77	105	2	103	.79	$\pm$.08	-.06	68	17	51	.14	$\pm$.03
.75	85	3	82	.63	$\pm$.07	-.10	49	16.5	32.5	.09	$\pm$.02
.73	71	2	69	.54	$\pm$.07	-.16	80	25	55	.08	$\pm$.01
.71	48	3	45	.35	$\pm$.06	-.24	58	14	44	.06	$\pm$.01
.69	33	2	31	.25	$\pm$.05	-.32	49	8	41	.06	$\pm$.01
.66	56	5	51	.20	$\pm$.03	-.40	39	6.6	32.4	.05	$\pm$.01
.62	41	5	36	.14	$\pm$.03	-.48	42	6.6	35.4	.06	$\pm$.01
.58	21	6	15	.06	$\pm$.02	-.56	30	6.6	23.4	.04	$\pm$.01
.54	32	6	26	.10	$\pm$.02	-.64	20	6.6	13.4	.02	$\pm$.01
.50	20	7	13	.05	$\pm$.02	-.72	11	5	6	.01	$\pm$.01
.46	27	8	19	.08	$\pm$.02	-.80	11	4.6	6.4	.01	$\pm$.01
.42	36	8	28	.11	$\pm$.03	-.88	16	4.6	11.4	.02	$\pm$.01
.38	51	9	42	.17	$\pm$.03	-.94	8	2.3	5.7	.03	$\pm$.02

TABLE V

COEFFICIENTS FOR POWER SERIES FIT

Coefficient	11th Order Fit With Forward Point	10th Order Fit Without Forward Point
A_0	.125 ± .010	.137 ± .009
A_1	.462 ± .066	.511 ± .060
A_2	.873 ± .301	.100 ± .273
A_3	- 2.71 ± 1.14	- 4.63 ± .832
A_4	-12.54 ± 2.44	- 4.22 ± 2.28
A_5	- 1.16 ± 6.87	15.48 ± 3.78
A_6	46.37 ± 7.61	14.27 ± 7.58
A_7	32.25 ± 17.84	-23.51 ± 6.63
A_8	-69.07 ± 9.87	-18.88 ± 10.91
A_9	-61.32 ± 20.51	17.88 ± 3.90
A_{10}	41.44 ± 4.47	14.42 ± 5.65
A_{11}	39.83 ± 8.54	----

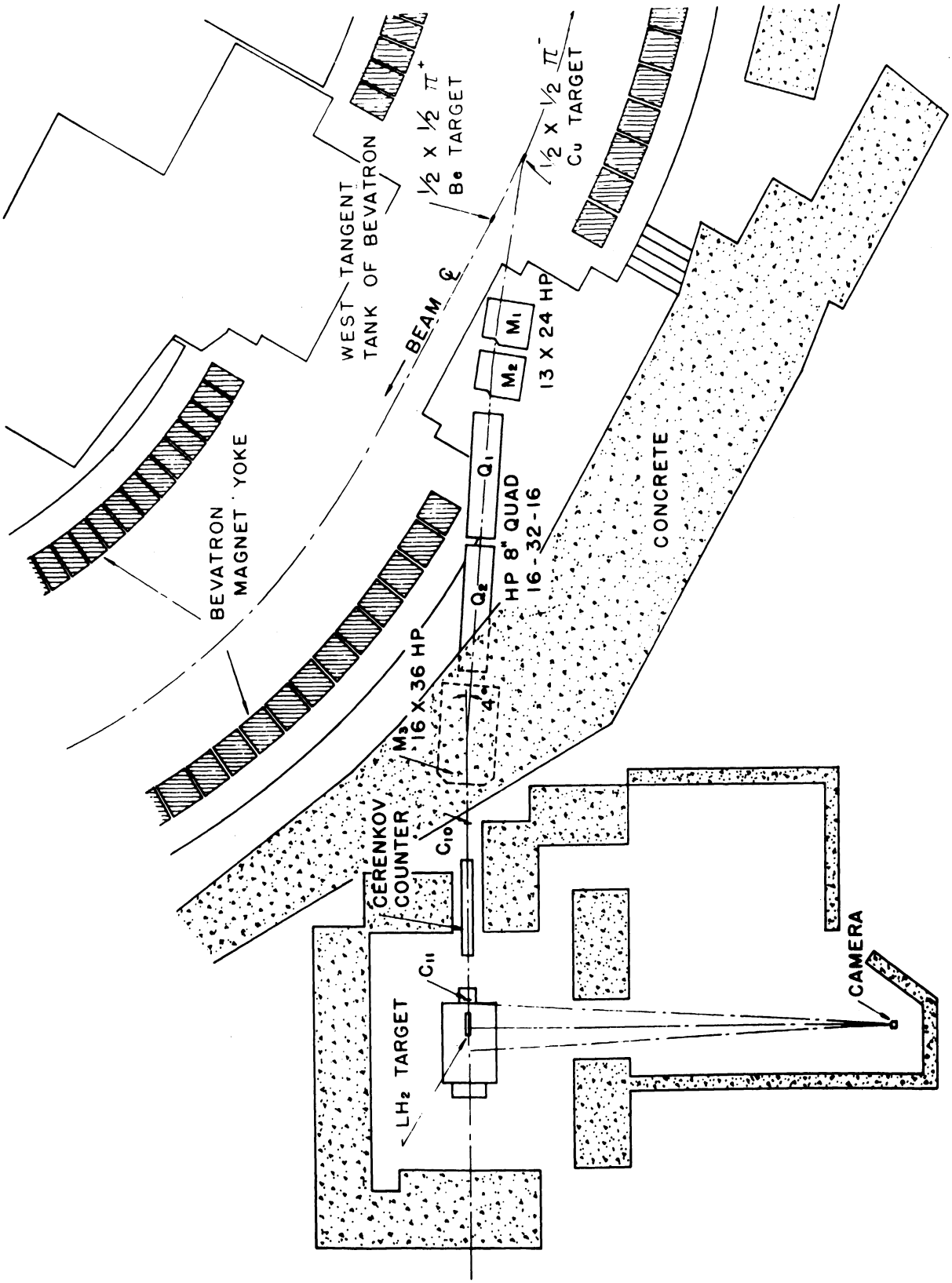

Fig. 1. The beam layout.

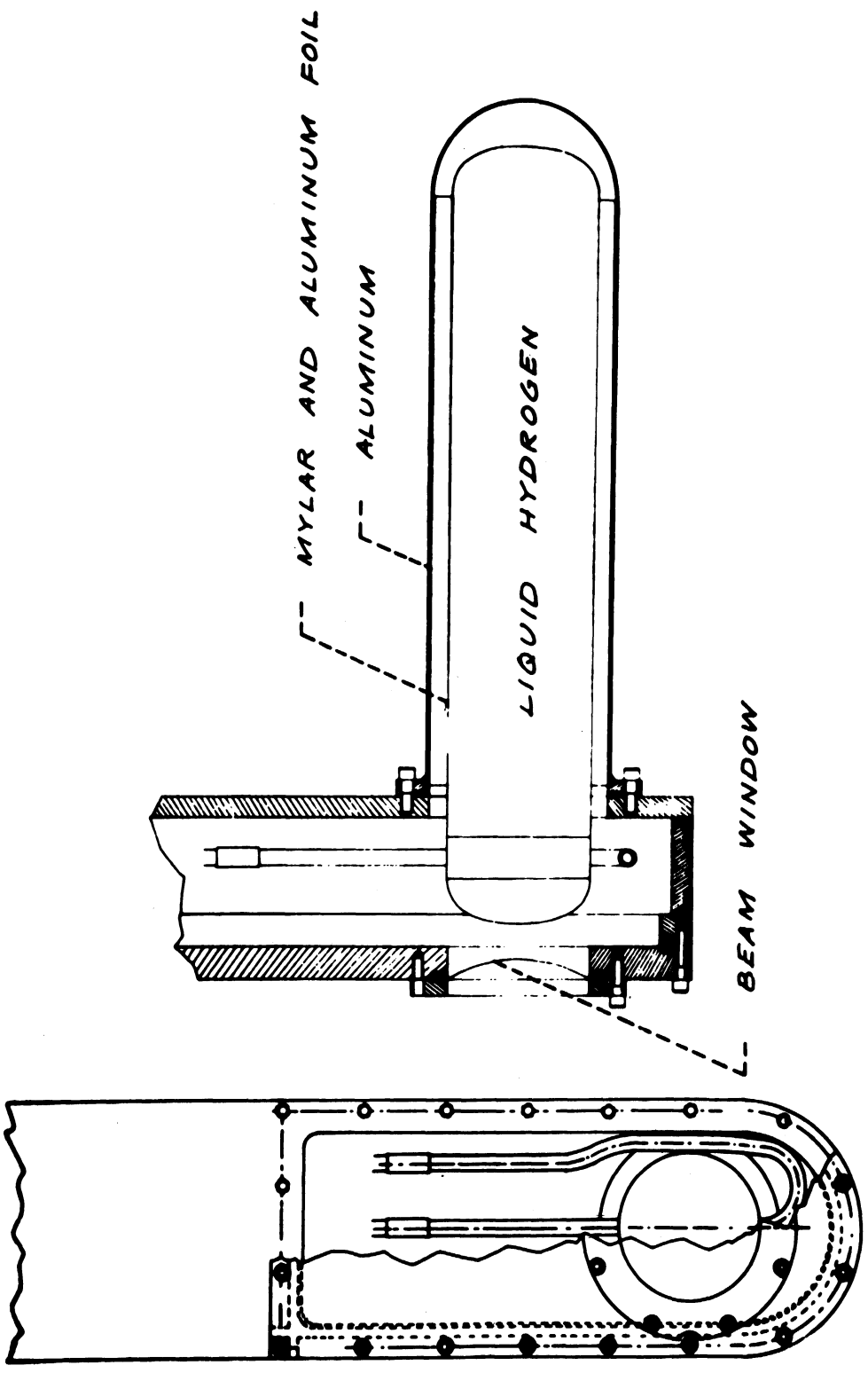

Fig. 2. The hydrogen target.

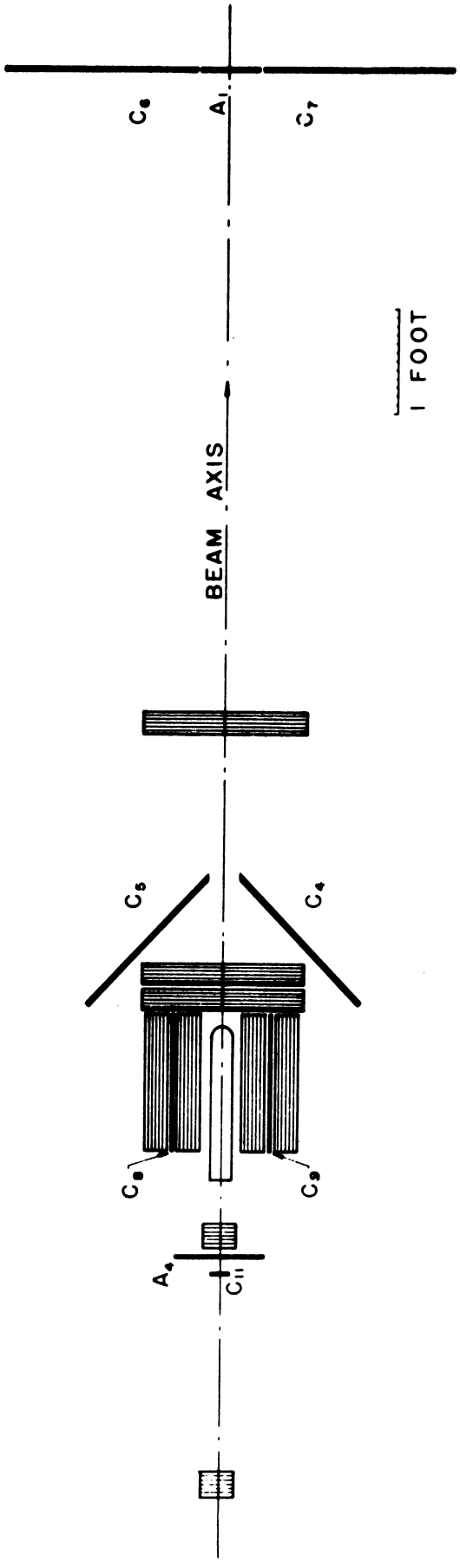

Fig. 3. Arrangement of spark chambers and counters.

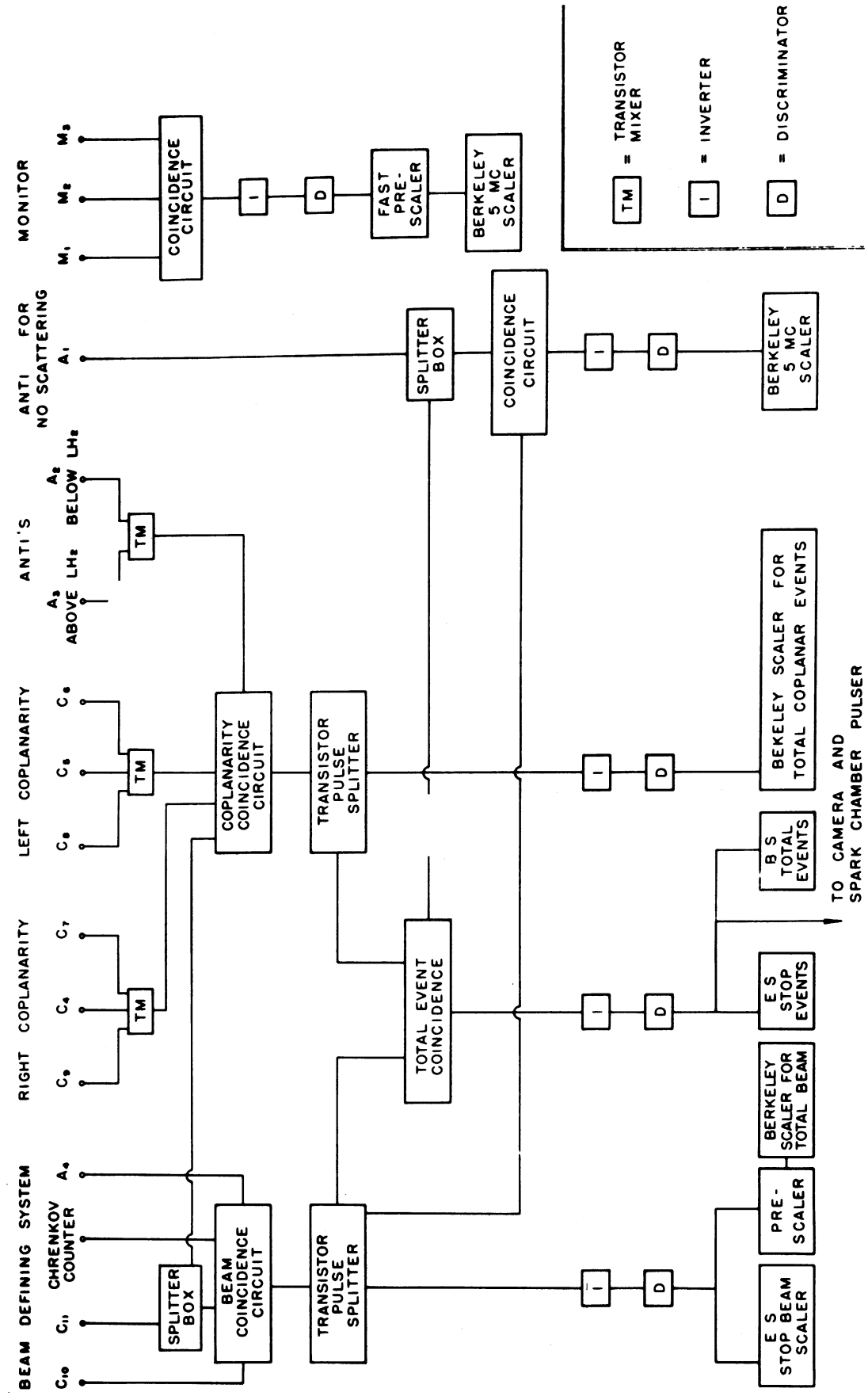

Fig. 4. Event detection electronics.

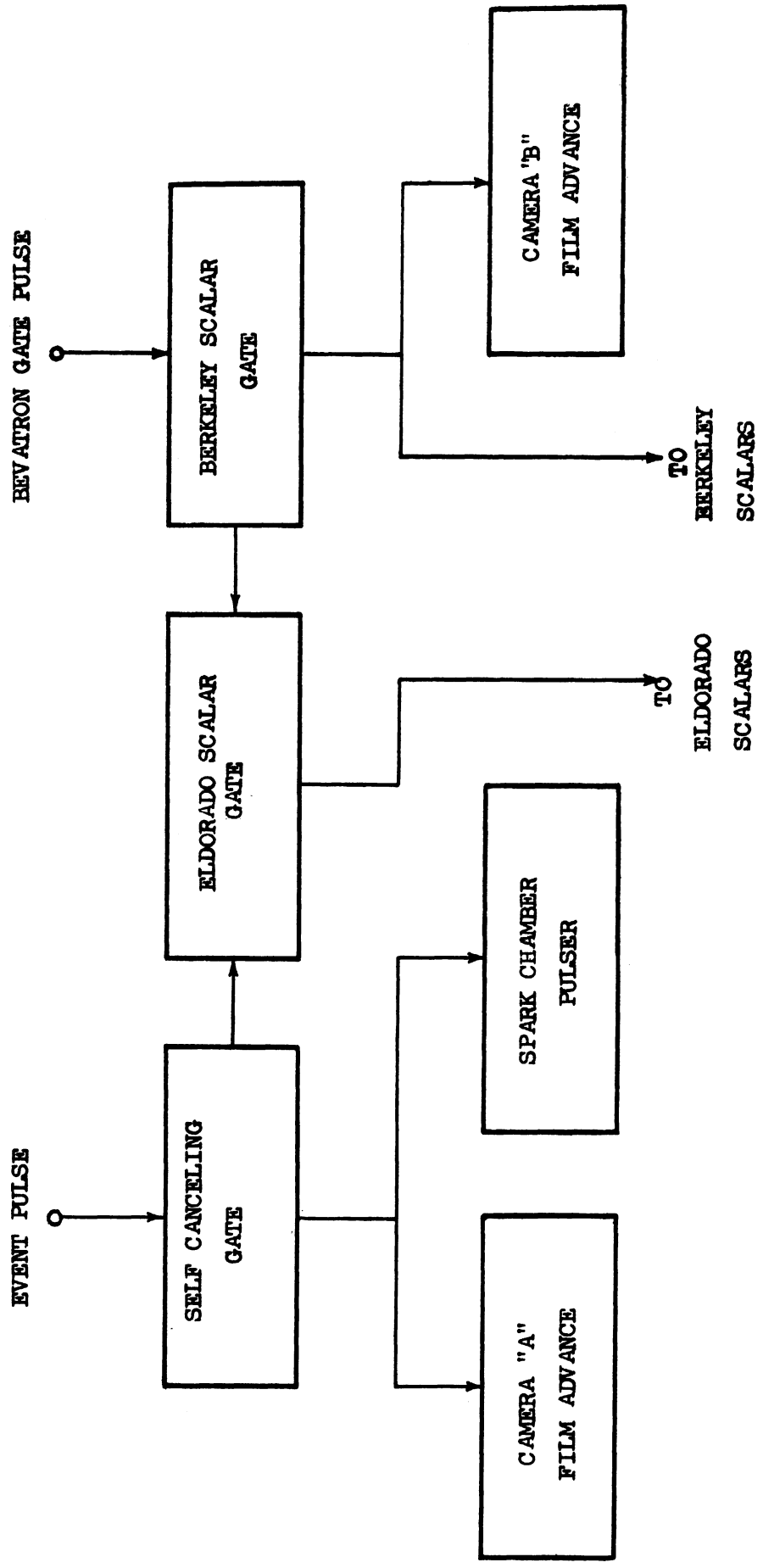

Fig. 5. Gate and film advance system.

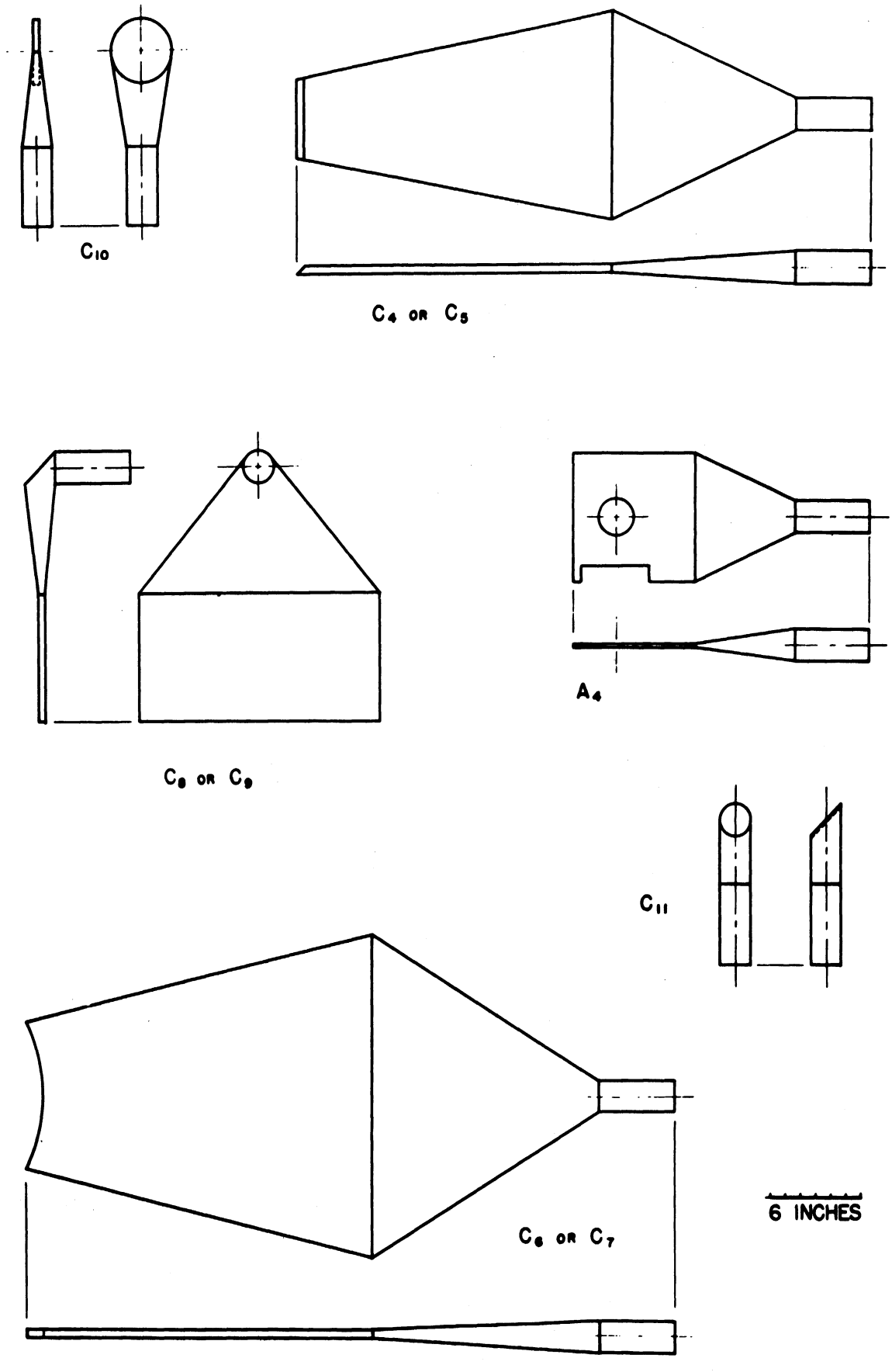

Fig. 6. Geometrical configuration of triggering counters.

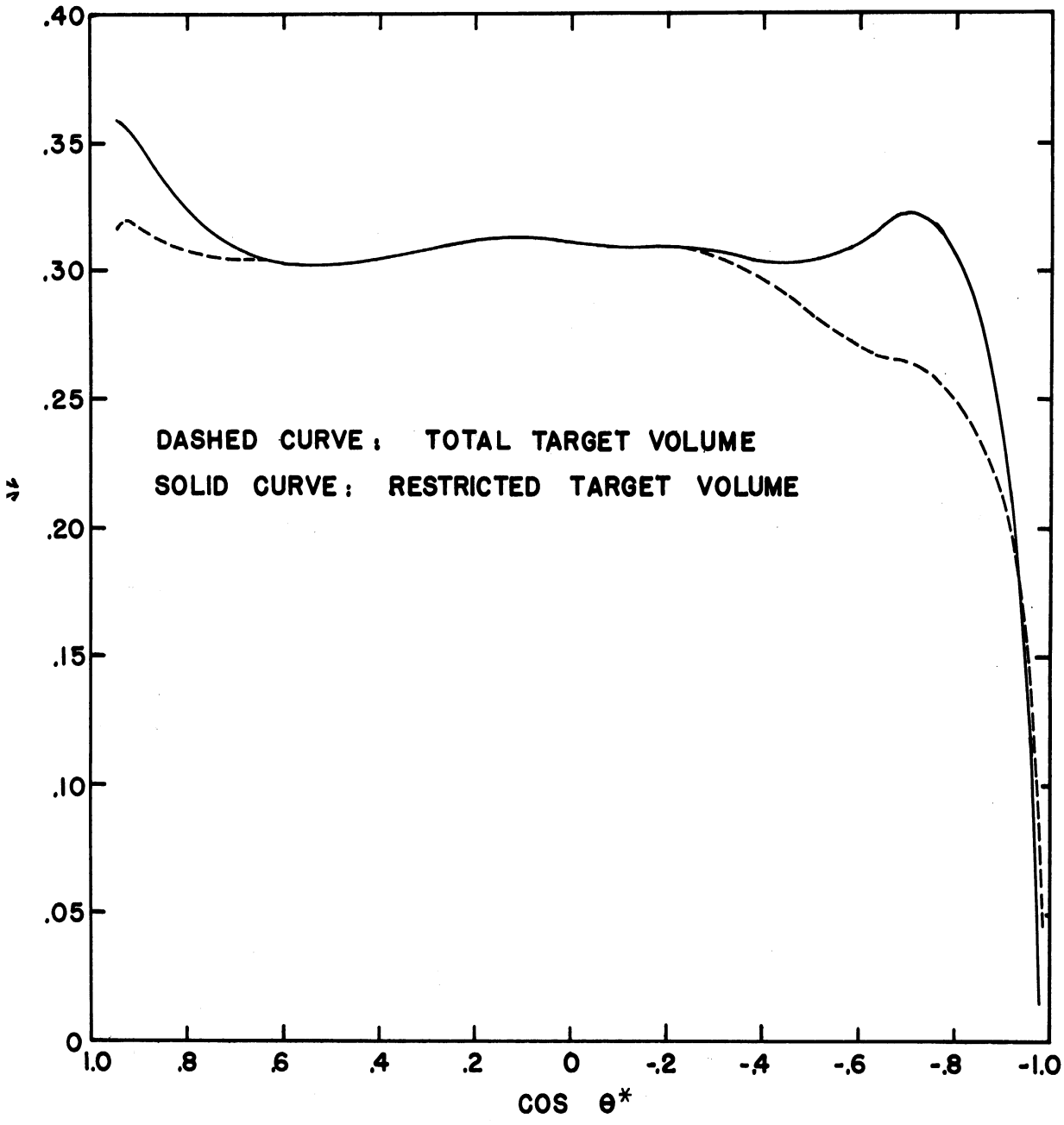

Fig. 7. Effective detection solid angle as a function of scattering angle.

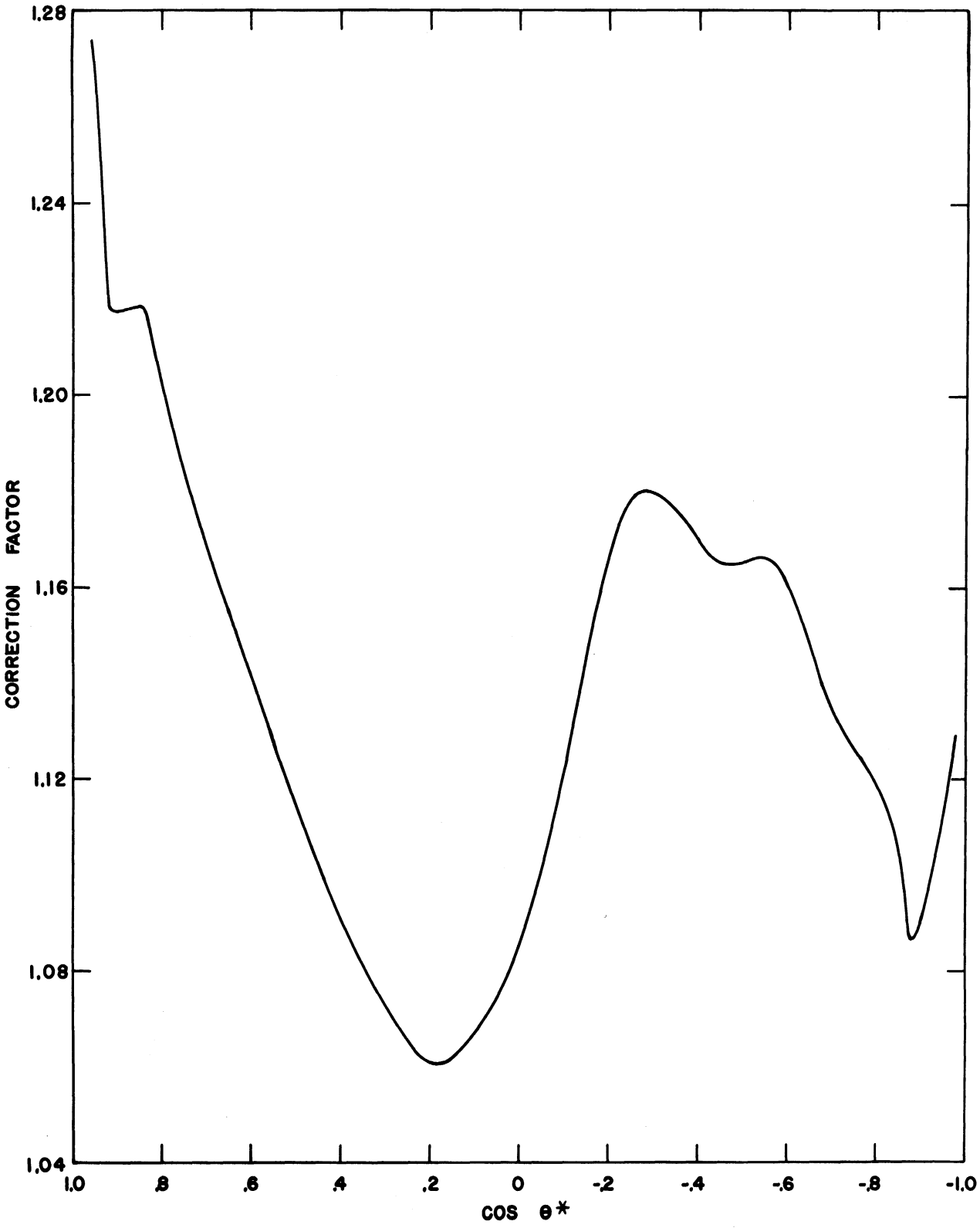

Fig. 8. Nuclear scattering and spark chamber solid angle correction (all events).

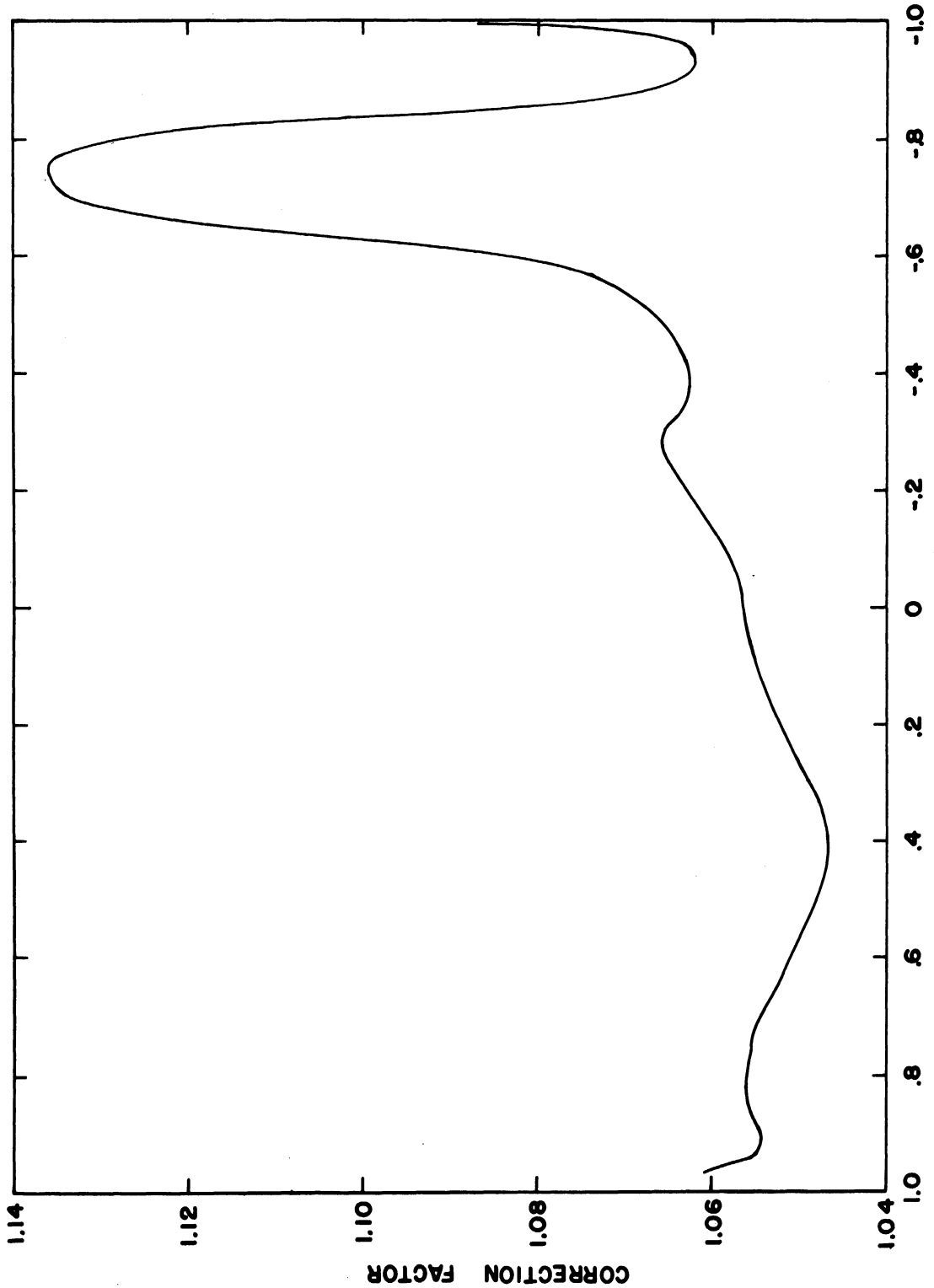

Fig. 9. Nuclear scattering and spark chamber solid angle correction (restricted target).

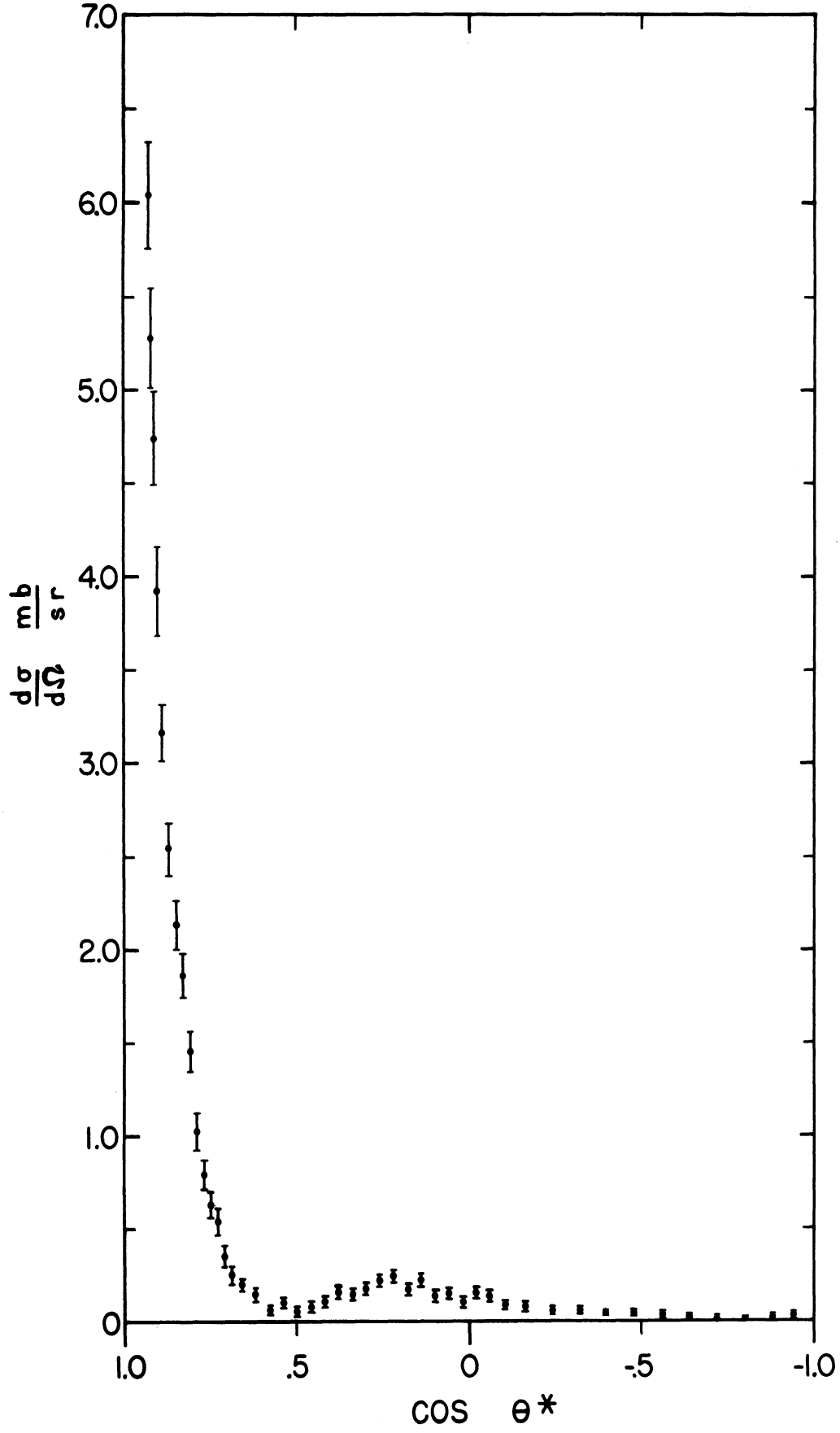

Fig. 10. Angular distribution (restricted target).

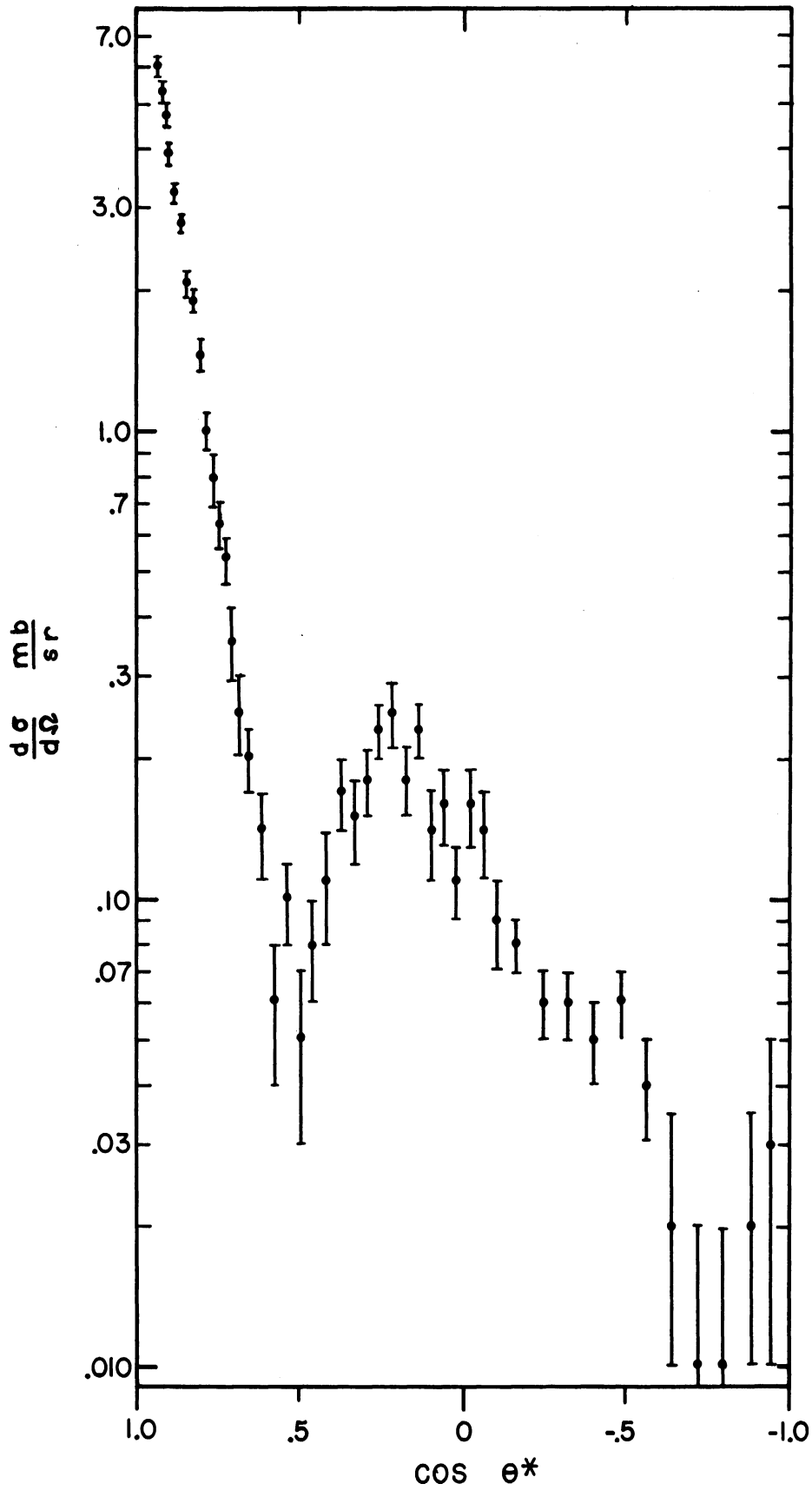

Fig. 11. Angular distribution (restricted target) on semi-log scale.

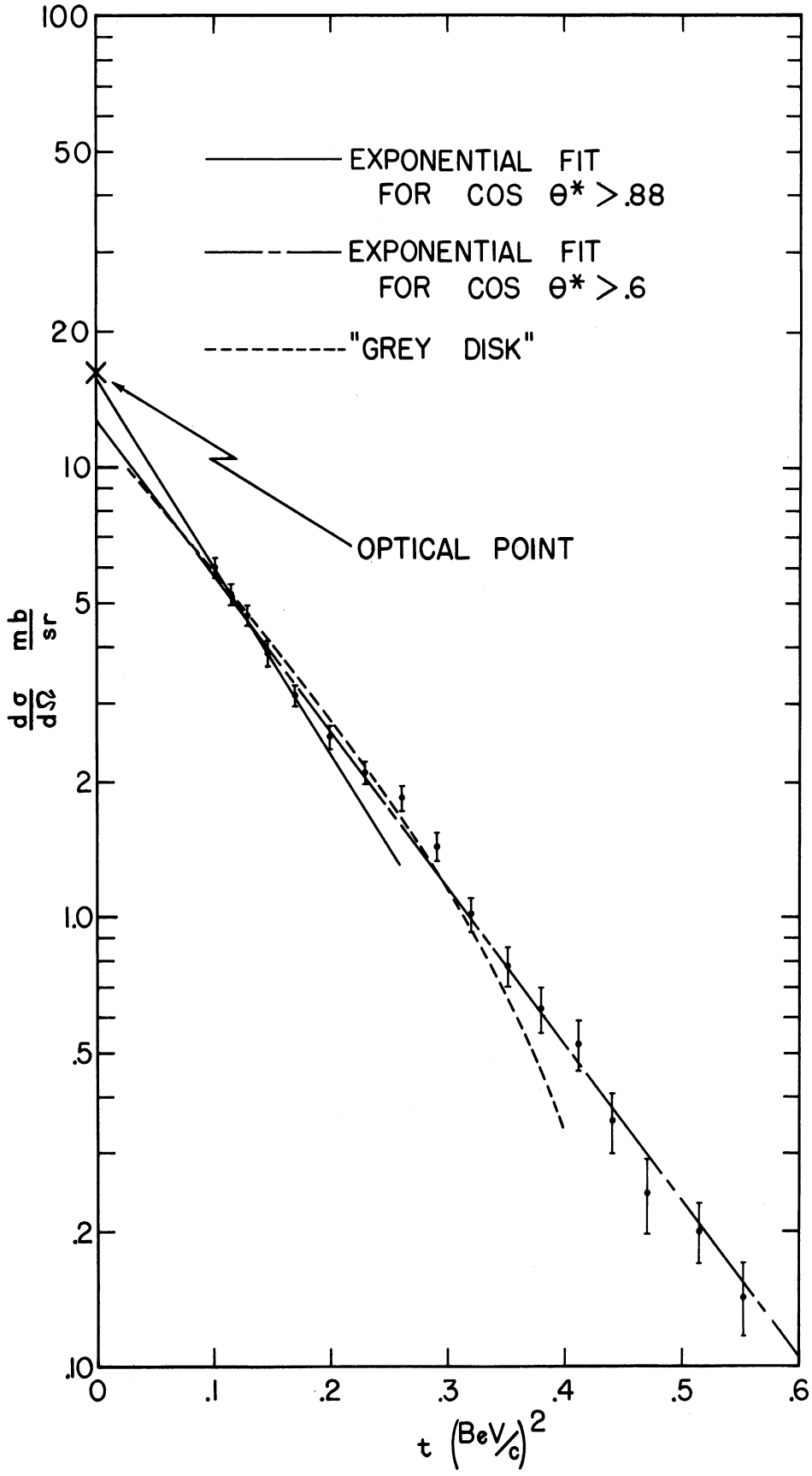

Fig. 12. The diffraction peak with various fitted curves.

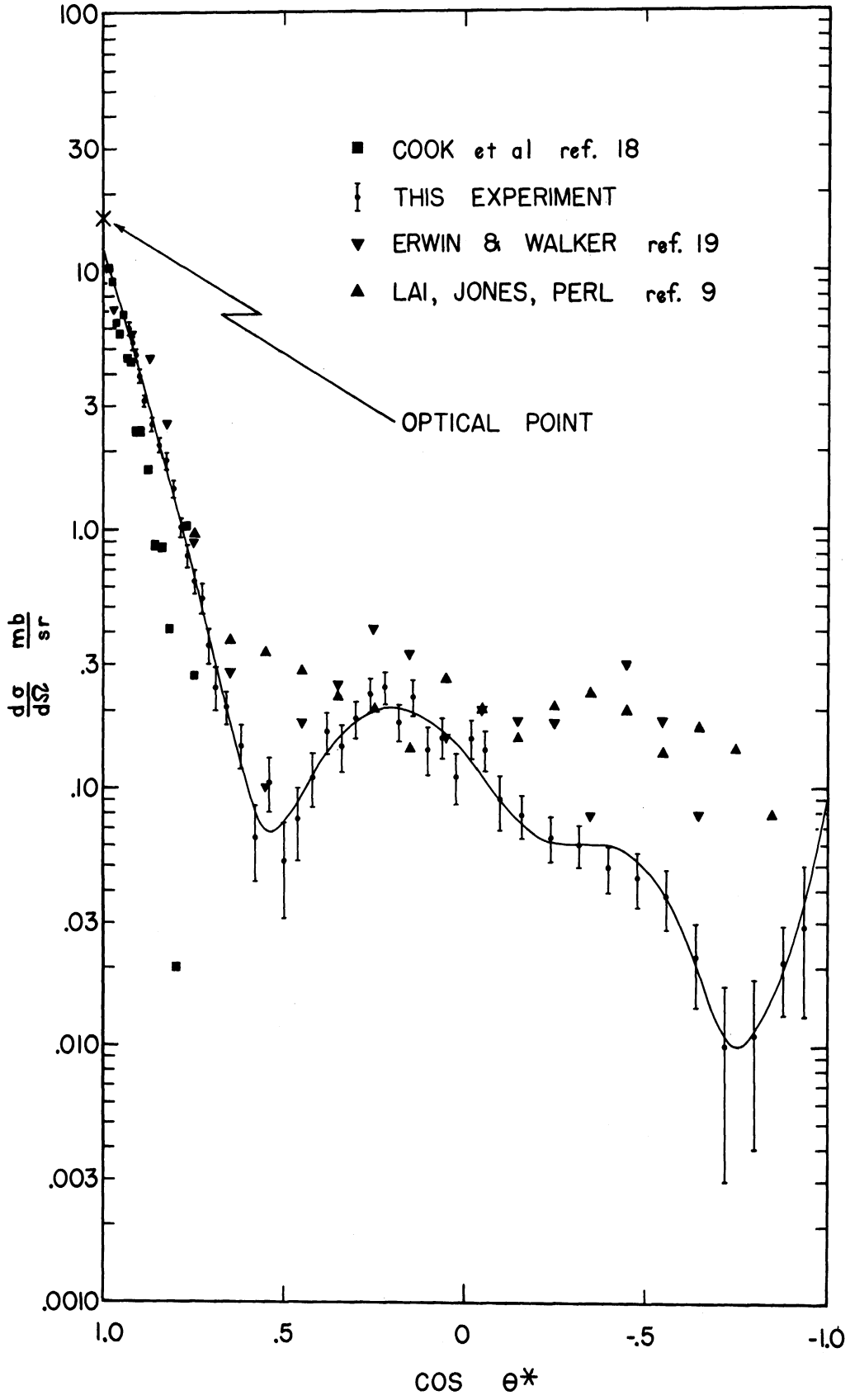

Fig. 13. A power series fit to the angular distribution with a comparison to other experiments.

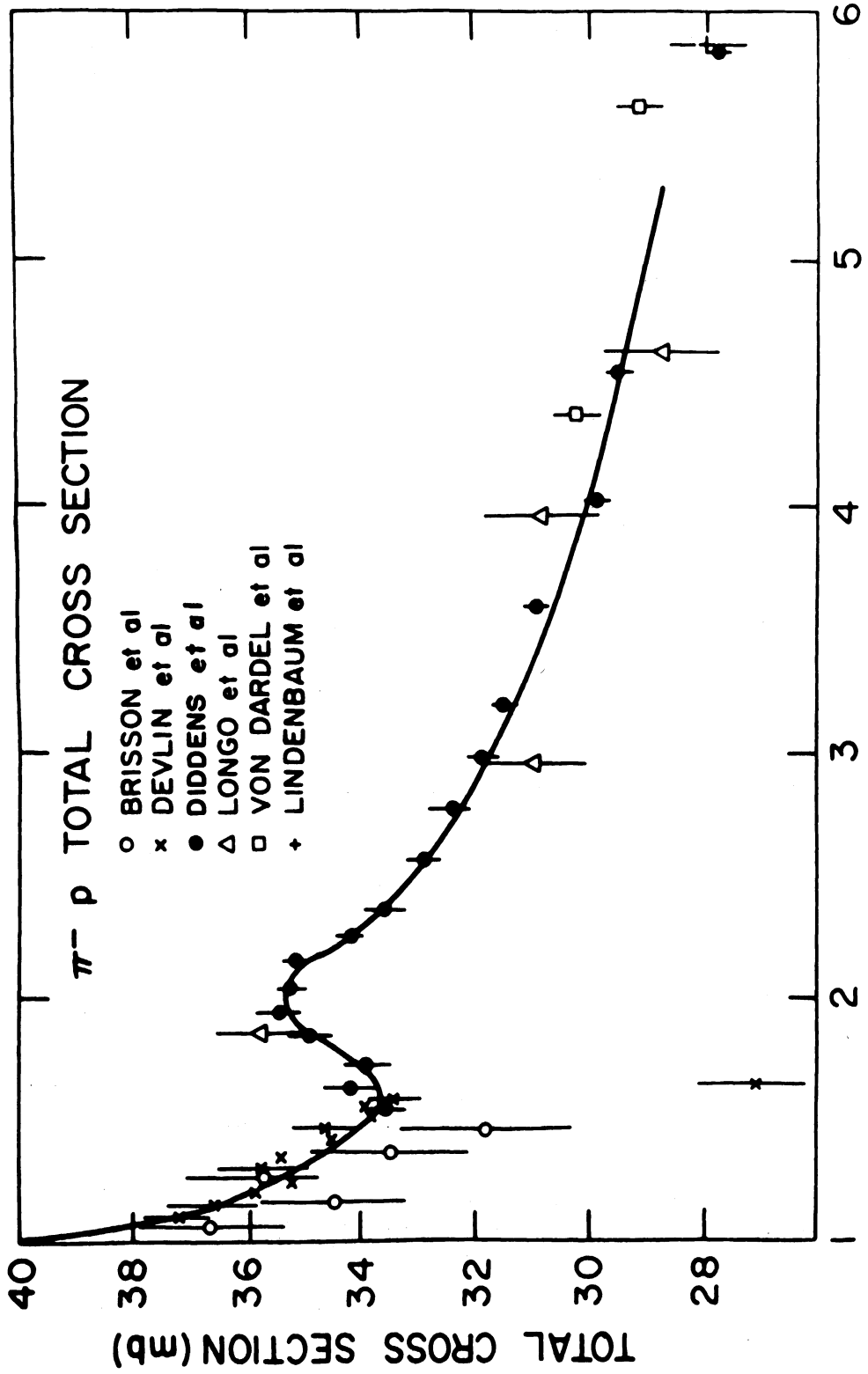

Fig. 14. Total negative pion-proton cross section from 1 to 6 Bev.

REFERENCES

1. K. W. Lai, L. W. Jones, and M. L. Perl, Phys. Rev. Letters 7, 125 (1961); K. W. Lai, thesis, University of Michigan, unpublished, 1962.

2. A. N. Diddens, E. W. Jenkins, T. F. Kycia, and K. F. Riley, Phys. Rev. Letters 10, 262 (1963).

3. L. D. Landau and E. M. Lifshitz, Quantum Mechanics (Addison Wesley, 1958), p. 436.

4. K. R. Greider and A. E. Glassgold, Ann. Phys. 10, 100 (1960).

5. T. Regge, Nuovo Cimento 14, 951 (1959); 18, 947 (1960).

6. S. C. Frautschi, M. Gell-Mann, F. Zachariason, Phys. Rev. 126, 2204 (1962).

7. K. J. Foley, et al., Phys. Rev. Letters 10, 376 (1963).

8. J. Helland, Doctoral thesis, University of California Radiation Laboratory Report UCRL-10378, published (1962).

   J. Helland, et al., Phys. Rev. Letters 10, 27 (1963).

   C. Wood, Doctoral thesis, University of California Radiation Laboratory Report UCRL-9507, unpublished (1961).

9. K. W. Lai, L. W. Jones, and M. L. Perl, Phys. Rev. Letters 7, 125 (1961); K. W. Lai, thesis, University of Michigan, unpublished, 1962.

10. Lawrence Radiation Laboratory Counting Handbook. Lawrence Radiation Laboratory Report UCRL-9054, unpublished, 1960.

11. D. Meyer and K. Terwilliger, Rev. Sci. Instr. 32, 512 (1961); J. Fischer and G. Zorn, Rev. Sci. Instr. 32, 512 (1961).

12. F. S. Crawford, et al., Phys. Rev. Letters 3, 394 (1959); S. E. Wolf, et al., Rev. Mod. Phys. 33, 439 (1961).

REFERENCES (Concluded)

13. L. O. Roelling and D. A. Glaser, Phys. Rev. 116, 1001 (1959).

M. Chrétien, J. Leitner, N. P. Samios, M. Schwartz, and J. Steinberger, Phys. Rev. 108, 383 (1957).

L. Bertanza, R. Carrara, A. Drago, P. Franzini, I. Mannelli, G. V. Silvestrini, and P. H. Stoker, Nuovo Cimento 19, 467 (1961).

V. Cook, B. Cork, T. F. Hoang, D. Keefe, L. Kerth, W. A. Wenzel, and T. F. Zipf, Phys. Rev. 123, 320 (1961).

R. Thomas, Phys. Rev. 120, 1915 (1960).

14. V. Cook, B. Cork, W. Holley, and M. L. Perl, to be published in Phys. Rev.

15. C. C. Ting, L. W. Jones, and M. L. Perl, Phys. Rev. Letters 9, 468 (1962).

C. C. Ting, Doctoral thesis, University of Michigan, unpublished, 1963.

16. R. C. Whitten and M. M. Block, Phys. Rev. 111, 1674 (1958).

17. L. P. Kotenko, et al., Soviet Physics-JETP 15, 800 (1962).

18. V. Cook, et al., Phys. Rev. 123, 320 (1961).

19. A. R. Erwin and W. D. Walker, unpublished data.

20. J. Alitti, et al., Nuovo Cimento 22, 1310 (1961).

UNIVERSITY OF MICHIGAN
3 9015 02526 7835